In-plane structure of magnetite thin films

Project thesis of

Yifan Xu

At the Jülich Center for Neutron Science,
Institute of Quantum Materials and Collective Phenomena
in Forschungszentrum Jülich

Supervisor：	Prof. Dr. Thomas Brückel
Advisors:	Dr. Mai Hussein Hamed Dr. Connie Bednarski-Meinke

2. February 2022 – 2. May 2022

Abstract

We observe the different in-plane orientations of Fe_3O_4 (111) magnetite thin films grown on Yttria-stabilized zirconia (YSZ) (001) by doing ϕ-scan (in-plane rotation scan). We grow Fe_3O_4 films by pulsed laser deposition (PLD). The quality of the magnetite films is checked by different techniques e.g. Atomic force microscopy (AFM), X-ray reflectometry (XRR). With X-Ray Diffraction (XRD), we observe the single orientation of Fe_3O_4 in out-of-plane direction. ϕ-scan by using 4Circle devices indicates the existence of four domains in in-plane, driven by the different orientation of thin films on the substrates. By wide angle X-ray scattering (WAXS), the single crystallinity is observed. Our study provides an insight for magnetite in-plane surfaces influenced by the substrates, which is a necessary step to understand their interfaces with other substrates in spintronic devices.

Überblick

Die unterschiedlichen *in plane* Orientierungen von auf YSZ (001) gewachsenen Magnetit-Dünnschichten wurden durch ϕ-Scans beobachet. Die Fe3O4 Filme wurden mittels gepulster Laserabscheidung (PLD) hergestellt. Die Qualität der Magnetitfilme wurde mit verschiedenen Techniken, z.B. Rasterkraftmikroskopie (AFM) und Röntgenreflektometrie (XRR) überprüft. Durch Röntgendiffraktion wurde eine einzige *out of plane* Orientierung beobachtet. Durch ϕ-Scans mit einem Vierkreisdiffraktometer konnte die Existenz von von vier Domänen in der Ebene gezeigt werden. Die Domänen sind durch abweichende Kationenbesetzungen in den Dünnschichten gegeben. Durch Weitwinkel-Röntgenbeugung (WAXS) konnte die Einkristallinität der Dünnfilme nachgewiesen werden. Die Studie bietet einen Einblick in den Einfluss des Substrates auf die *in plane* Struktur von Magnetitoberflächen und trägt zum Verständnis von Magnetit/Substrat Grenzflächen in spintronischen Komponenten bei.

Contents

Chapter 1

Introduction and motivation

Iron oxides have drawn a lot of interest in numerous fields. Fe_3O_4 magnetite is an important magnetic material which has been used for thousands of years. The half-metallic Fe_3O_4 has a high Curie temperature ($T_C = 860K$), which allows it to be used at room temperature. It has been applied in many technological such as spintronic devices, magnetic recording media, etc [1]. The growth and properties of magnetite thin films have been studied in the past two decades [2]. Thousands of studies have been focused on understanding the high Curie temperature, first-order Verwey transition character in magnetite in order to make it suitable in the application of spintronic device in the form of thin films [3].

Influenced by the substrate and growth parameters, Fe_3O_4 thin films can align in different planes on the substrates including (100), (111), (110), (311), (331), and (511) [4] - among them the (100) surface has been thoroughly investigated [5]. In this study, we have chosen to study the Fe_3O_4 (111) plane induced by the orientation of thin films on the YSZ substrates. The three-fold Fe_3O_4 (111) plane has been reported in the last century [6]. In this study, we aim to study the influence of the orientation of thin films on the substrate and to investigate the in-plane structure of Fe_3O_4 (111) thin films on the YSZ (001) substrates.

In chapter 2 the scientific background of Fe_3O_4 magnetite will be introduced. Additionally, the lattice structure of the YSZ substrates and the possible growth mode are introduced. Also, we introduce the scattering from thin films including reflection and diffraction.

The experimental methods and instruments used for the deposition, characterization of the in-plane and out-of-plane properties of the thin films will be introduced in chapter 3.

In chapter 4, the pulsed laser deposition (PLD) has been introduced to grow the thin films. The quality of the thin films is checked by the roughness calculated from XRR data. With XRD, we study the out-of-plane structure of Fe_3O_4 (111) thin films. Finally, the in-plane structure is studied with the 4-Circle instrument and WAXS where we observe the different domains in the Fe_3O_4 (111) plane.

In chapter 5, we summarize the outcomes of this study. The direction of further study is discussed in chapter 6.

Chapter 2

Theory

In this theoretical background section, the properties of magnetite will be first introduced. Depending on the lattice mismatch, the growth mode of magnetite thin films on YSZ substrates will be discussed in section 2.2. In section 2.3, we will introduce the X- ray scattering from thin films.

2.1 Magnetite (Fe_3O_4)

Magnetite Fe_3O_4 is a ferrimagnetic half-metal which has been studied over thousands years because of its special properties [7].

2.1.1 Structure

Fe_3O_4 has a cubic inverse spinel structure, with a crystal lattice constant of 8.394Å, as shown in Figure 2.1a [8]. All of the Fe^{2+} ions occupy half of the octahedral sites and the Fe^{3+} are split evenly across the remaining half of octahedral sites and the tetrahedral sites. The magnetic moment at octahedral sites and tetrahedral sites are with different orientation. Thus, this pattern of occupation of Fe^{2+} and Fe^{3+} cations causes the special ferrimagnetic and electric properties of magnetite.

2.2 Epitaxial growth of Fe_3O_4 on YSZ substrates

Different substrates have different oxygen supply characters. For example, Strontium titanate can oxidize Fe_3O_4 and supply oxygen to the thin films which will influence the iron oxide phases [9]. Yttria-stabilized zirconia (YSZ) is chosen as oxide substrate, which has “inert” oxygen supplying properties. In other words, YSZ as a substrate doesn’t supply oxygen to Fe_3O_4 thin film.

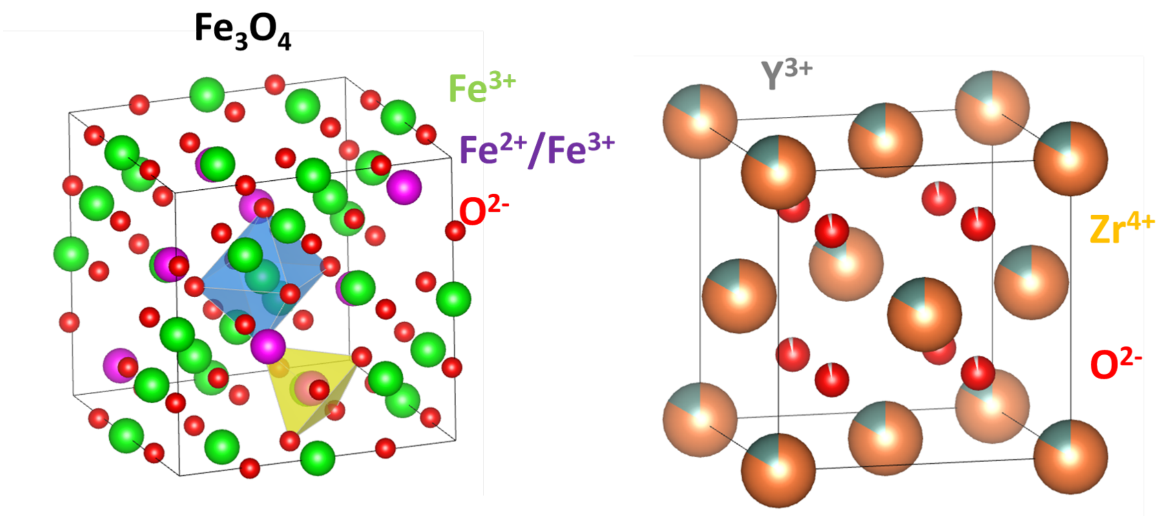

(a) Fe_3O_4 crystal structure and the tetrahedra/ Octahedra coordination polyhedron structure

(b) YSZ crystal structure

Figure 2.1: The unit cells of (a) Fe_3O_4 and (b) YSZ

2.2.1 YSZ crystal structure

The main phase of YSZ is ZrO_2, which is monoclinic at room temperature and unstable cubic at 2370 °C. It is stabilized by doping with 9.5 mol% Y_2O_3 to reach a stable cubic structure at room temperature. YSZ is an insulator with a face centered cubic structure and a lattice constant of 5.16Å.

2.2.2 Growth modes of thin films

Due to the lattice mismatch, there is strain induced by substrate during the film deposition. Depending on the relationship between the lattice constant of the thin film a_{Film} and of the substrate $a_{Substrate}$, the thin films growth mode can be different [10].

Epitaxial films

Epitaxial growth means the continuation of the alignment of the single crystal substrate into the crystalline film. The substrate offers a template for positioning the atoms of film materials and this pattern will be adapted in the further growth. Epitaxial growth is determined by the structure and the energy between the interface of films and substrates. It can happen when the lattice mismatch of the thin film and substrate is not large ($<15\%$) [11]. When the lattice mismatch is less than 0.5%, the growth tends to be planar. If the lattice mismatch is larger, the material tends to grow by island mode but still epitaxially [12]. For the parallel epitaxial film, we will only see one set of peaks in a diffraction pattern in both the in-plane and out-of-plane direction, which is because of the single orientation of the crystal on the substrate.

Textured films

Texture means there is an anisotropic distribution of the crystallities in the thin films. It can be due to templating from the crystalline orientation of the substrate. It can be mono-axially textured in out-of-plane and have different orientation in in-plane [10].

Randomly-oriented polycrystalline films

Growth of polycrystalline films always begins with the nucleation of the island. Polycrystalline films with no preferential orientation should have the same intensity in XRD as the powder diffraction pattern.

2.2.3 Epitaxial growth of Fe_3O_4 on YSZ substrates

The lattice constants of Fe_3O_4 and YSZ are $8.395\mathring{A}$ and $5.16\mathring{A}$, respectively. The YSZ (001) and Fe_3O_4 (001) planes are shown in Figure 2.2a and 2.2b. The lattice mismatch between Fe_3O_4 (001) and YSZ (001) can be calculated:

$$\varepsilon = \frac{a_{Fe_3O_4} - a_{YSZ}}{a_{YSZ}}$$

$$\varepsilon = \frac{5.94 - 5.16}{5.16} = 15.12\%$$

This high mismatch is not energetically favorable and Fe_3O_4 film tends to grow parallel to the (111) planes [14]. The Fe_3O_4 (111) plane is shown in Figure 2.2c. Fitting Fe_3O_4 (111) on YSZ (001) means matching a 3-fold pattern to a 4-fold base. A possible solution is to determine the most similar

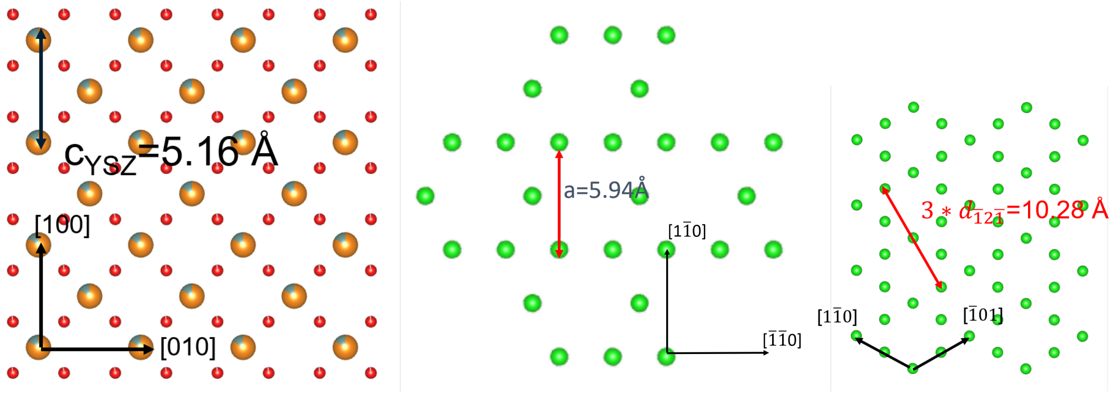

(a) YSZ (001) plane **(b)** Fe_3O_4 (001) plane **(c)** Fe_3O_4 (111) plane

Figure 2.2: Sketch of YSZ (001) plane and Fe_3O_4 plane drawn by VESTA [13]. Yttrium ions in grey, zirconium ions in orange oxygen ions in red and iron ions in green.

interplanar spacing in Fe_3O_4 (111) plane as the lattice constant of YSZ. The interplanar spacing between $(\bar{1}2\bar{1})$ planes ($d_{\bar{1}2\bar{1}}$) can be calculated using the Miller indices:

$$d_{hkl} = \frac{a}{h^2 + k^2 + l^2}$$

$$d_{\bar{1}2\bar{1}} = \frac{8.395}{(-1)^2 + 2^2 + (-1)^2} = 3.43\mathring{A}$$

Three of the $d_{\bar{1}2\bar{1}}$ repeats itself over the distance. Thus, 2 of the YSZ unit cell can fit one of the repetation in Fe_3O_4 (111) plane. This occupation can be represented as $(111)\langle\bar{1}2\bar{1}\rangle_{Fe_3O_4} \| (001)\langle 100\rangle_{YSZ}$. The mismatch ($\varepsilon$) in between can still calculated by the interplanar spacing (d) [15]:

$$\varepsilon = \frac{3 * d_{\bar{1}2\bar{1}} - 2 * a_{YSZ}}{2 * a_{YSZ}}$$

$$\varepsilon = \frac{3 * 3.43 - 2 * 5.16}{2 * 5.16} = -0.3\%$$

The new mismatch between the Fe_3O_4 (111) and YSZ (100) is only -0.3%, which is acceptable for heteroepitaxial film growth.

2.3 Scattering from thin films

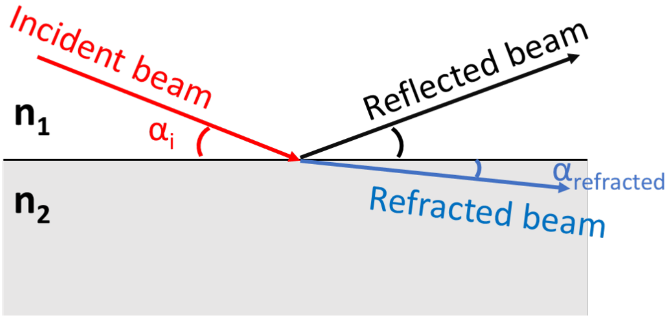

Figure 2.3: Reflection and refraction of X-ray

The incident X-Ray can be either reflected or refracted by a thin film system as shown in Figure 2.3. In this section, two different scattering methods used in this thesis, reflectometry and diffraction, will be introduced.

2.3.1 Reflectometry

Reflectometry is scattering under grazing incidence. The incident X-ray goes through slits and is reflected by the surface of the thin film and the interface between the thin film and substrate as shown in Figure 2.5. X-ray reflectometry is surface sensitive. When the surface is not perfectly smooth, the

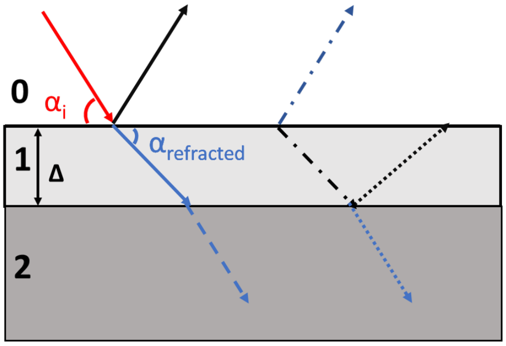

Figure 2.4: Constructive interference in a single thin film system

reflected angle will be deviate from the incident angle and there is no constructive interference. Thus, the intensity of the reflected beam, which is collected by the detector, will drop down.The deviations can then be analyzed to obtain the roughness of the surface.

As shown in Figure 2.5, the relation between incident and refracted X-Ray beam is:

$$n_1 cos(\alpha_i) = n_2 cos(\alpha_{refracted}) \tag{2.1}$$

The index of refraction of most materials is smaller than one, the index of refraction of air is equal to one. As a result, when we consider an X-Ray beam incident from the air and refracted in a thin film, then there would be a critical angle α_c for the incident beam. When the incident angle α_i is smaller than α_c there is no refraction, which is called “total internal reflection”. For a Fe_3O_4 thin film, α_c = 0.2°.

For a single thin film system, the refracted beam will be reflected at the interface between the substrate and thin film, then constructive interference occurs with the reflected beam at the surface of the thin film, as shown in Figure 2.5. This phenomenon causes the oscillation pattern called “Kiessig fringes”. By analyzing the period of these oscillations, thin film layer thickness and interlayer roughness can be determined. X-ray reflectivity measurements are often analyzed by fitting the measured data to a simulated curve. Fitting parameters are layer thickness, densities, roughness. Here, the program GenX [16] is used for analysis.

2.3.2 Diffraction

X-Ray diffraction is a common method to study crystalline materials. The crystal atoms scatter incident X-rays with the incident wavelength equals to the final wavelength, this phenomenon is called elastic scattering. The constructive or destructive interference can then cause the different intensities. In X-Ray diffraction methods, the angle and the intensity of the beam are measured.

Based on Bragg’s law (formula 2.2), incident X-rays show an interference pattern after interaction with the crystal lattice. The lattice constant d is easily calculated:

$$2dsin\theta = n\lambda \tag{2.2}$$

λ: the wavelength of X-ray, which is $1.54\AA$ in our instrument

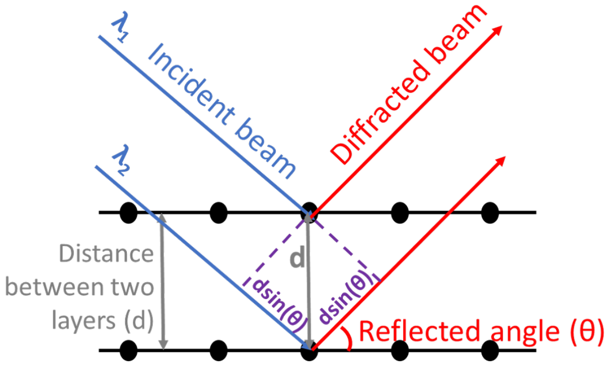

Figure 2.5: Bragg's law

The Laue oscillations occur when the Laue equations are fulfilled. Laue equations relate incoming waves to outgoing waves in the process of elastic scattering by a crystal lattice [17]. These Laue oscillations, due to the finite thickness of the film diffracting the incoming beam, are indicative of the films smooth interfaces and very high crystalline quality. From Laue oscillations the film thicknesses t can be determined with Formula 2.3, where λ is the wavelength of the X-rays , θ_{i+1} and θ_i are two adjacent maxima in the oscillations [18]. With this formula we can calculate the thickness of the crystalline part in thin films:

$$t = \frac{\lambda}{2(sin\theta_{i+1} - sin\theta_i)} \tag{2.3}$$

2.3.3 Two-dimensional diffraction

With two-dimensional diffraction, we can investigate both in-plane and out-of-plane structures at the same time. By plotting the data in a reciprocal space map, we can extract information from the X-ray diffraction pattern in detail. This detail can include the deviation from the perfect crystal structure allowing us to understand the different in-plane and out-of-plane strain state which can influence the physical properties the thin film [19].

The vector $\underline{r}^*$(hkl) from the origin to the reciprocal lattice point (h,k,l) is normal to the (hkl) plane of the crystal lattice. Every point in reciprocal space represents a possible reflection from the crystal lattice. Moreover, the length of the vector $\underline{r}^*$(hkl) is the reciprocal of the spacing of the (hkl) planes in real space. Thus, the nth point from the origin in a given row in the reciprocal lattice corresponds to the nth order reflection from the (hkl) crystal planes.

Not all the points in reciprocal space correspond to a reflection, to do so, they should also fulfill Bragg's equation. This phenomenon is described by Ewald's sphere. As shown in Figure 2.6, the incident and diffracted wave are given by $\underline{k_i}$ and $\underline{k_f}$, respectively. For the case of elastic scattering,

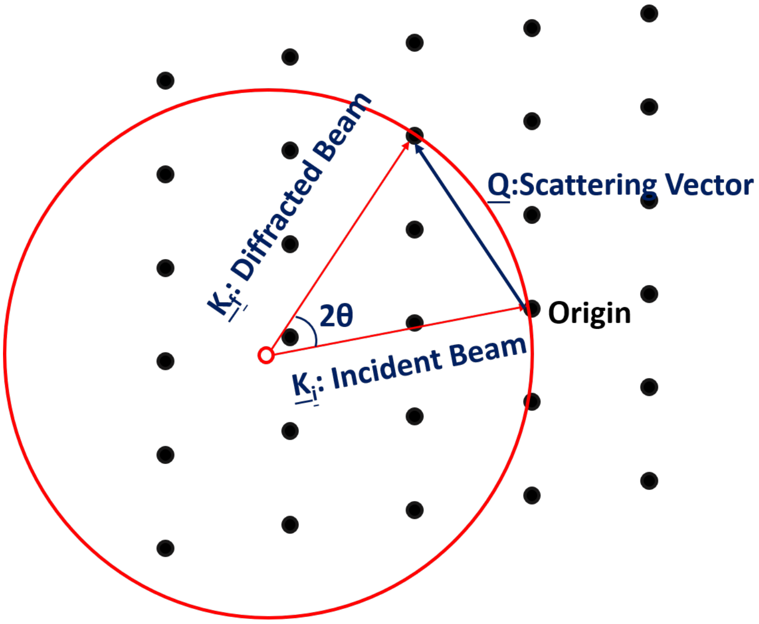

Figure 2.6: Illustration of diffraction using Ewald's sphere

both vectors have the same length which is reciprocal to the wavelength: $|\underline{k_i}| = |\underline{k_f}| = 1/\lambda$. The scattering vector $\underline{Q}$ is given by the difference between two vectors as shown in equation 2.4.

$$\underline{Q} = \underline{k_f} - \underline{k_i} \quad |\underline{Q}| = 2sin\theta/\lambda \tag{2.4}$$

With $|\underline{Q}| = |d^*_{hkl}| = 1/d_{hkl}$, we can fulfill Bragg's equation:

$$|\underline{Q}| = 2sin\theta/\lambda = 1/d_{hkl} \quad \lambda = 2d_{hkl}sin\theta \tag{2.5}$$

All possible $\underline{k_f}$ describe a sphere with a radius of $2\pi/\lambda$, which is Ewald's sphere. When the endpoint of $\underline{k_f}$ lies at a reciprocal lattice point hkl, the diffraction happens.

Chapter 3

Experimental methods

This study aims to study the in-plane structure of Fe_3O_4(111) thin films on YSZ(001) substrate. Pulsed laser deposition (PLD) is used to prepare the sample. The X-ray reflectometry provides the information of surface roughness of the thin film. The X-ray diffractometry offers the structure information in the out-of-plane direction. By using 4-Circle, the ϕ-scan is done to analyze the in-plane orientation. By using wide angle X-ray scattering, the different strain state can be studied. The details about the instruments used for preparation and characterization of the sample will introduced in this chapter.

3.1 Pulsed laser deposition (PLD)

Pulsed laser deposition (PLD) is a physical vapor deposition (PVD) technique that is widely used to deposit thin films on substrates. In a vacuum chamber, a high-power pulsed laser beam is focused on a target, and therefore, ablating the target material.

The vaporized target material deposits as a thin film on the substrates. This deposition occurs in the presence of a background gas– in our case, oxygen, which is commonly used when depositing oxides to fully oxygenate the deposited films. The deposition parameters influence the quality of the crystallization of thin films.

Our PLD process has the following parameters: a 50W KrF excimer laser with a pulse width of 25ns and a wavelength of λ=248nm is used. As shown in Figure 3.1, the high-power laser pulse is focused in a vacuum chamber on the rotating target. The material of the target (here Fe_2O_3) is vaporized to form a plasma plume. The ablated material consists of the neutral and ionized species, and then this material is directed to a substrate, which is 50 mm away from the target. The laser fluence F, which is calculated by the energy of laser pulses and the size of the laser spot on the target, is important for the ablation process. The laser fluence and the pulse repetition rate can be adjusted between F = 1-3 J/cm^2 and f = 1-50 Hz, respectively.

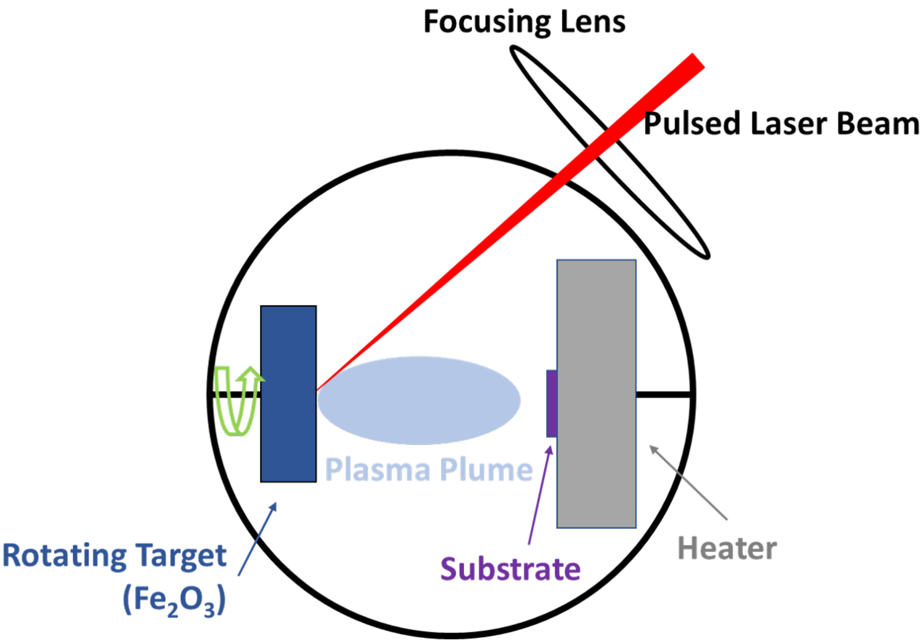

Figure 3.1: Sketch of PLD process

The film does not necessarily have the same composition as the target. In order to deposit Fe_3O_4 thin films, we choose the stable phase Fe_2O_3 as the target material. By changing the background oxygen pressure, the desired film stoichiometry can be reached. In this study, the base oxygen pressure is $1x10^{-7}$ mbar and the pressure during deposition is $2x10^{-6}$ mbar. In addition, the substrate is mounted on a heater which can reach a maximum of 850°C. By controlling the heater temperature, sufficient energy can be introduced for adatoms to diffuse and arrange themselves to form the desired crystalline structure

3.2 X-Ray Reflectometry/ Diffractometry (XRR and XRD)

X-Ray Reflectometry is a sensitive tool to characterize the surface of a thin film, here Bruker D8 Advance from PGI-7 (thanks to Prof. Dittmann) is used. A Cu-source is used as an X-ray source with a wavelength λ=1.54$\AA$.

3.3 4-Circle

The ϕ-scans are done using a Huber 4-circle diffractometer with a Cu-K_α tube at 40kV 40mA with a twin Göbel mirror setup for horizontal and vertical collimation. The beam size is around $0.5*0.5mm^2$.

Here we define the angle which between the incident beam and the detector arm as 2θ. The angle turns the sample holder around the same axis is defined as θ. The axis perpendicular and attached

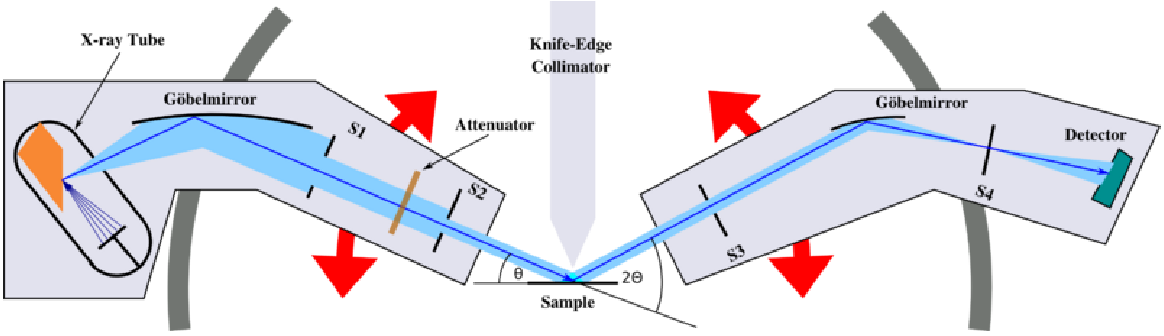

Figure 3.2: Sketch of D8 XRR (figure taken from ref. [29])

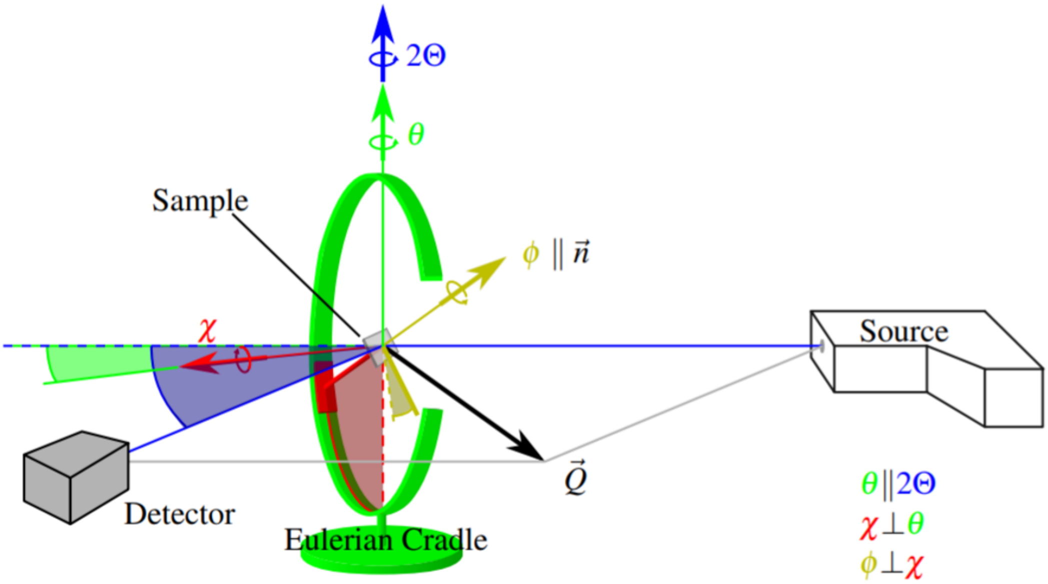

Figure 3.3: Sketch of 4-Circle (figure taken from ref. [29])

to θ is χ. The in-plane rotation angle of the sample is defined as ϕ [29]. The limit for the angle is different:

2θ-circle: 0-155°

θ-circle: -90-95°

χ-circle: -1.6-158.4°

ϕ-circle: 360°

The two further degrees of freedom of the 4-circle (χ and ϕ) allows measurement of the symmetry equivalent reflections in a chosen reflection family as shown in Figure 3.3. In Bragg geometry, (111) and (004) reflections of Fe_3O_4 are used to fit the lattice parameter.

3.4 Wide-Angle X-ray Scattering (WAXS)

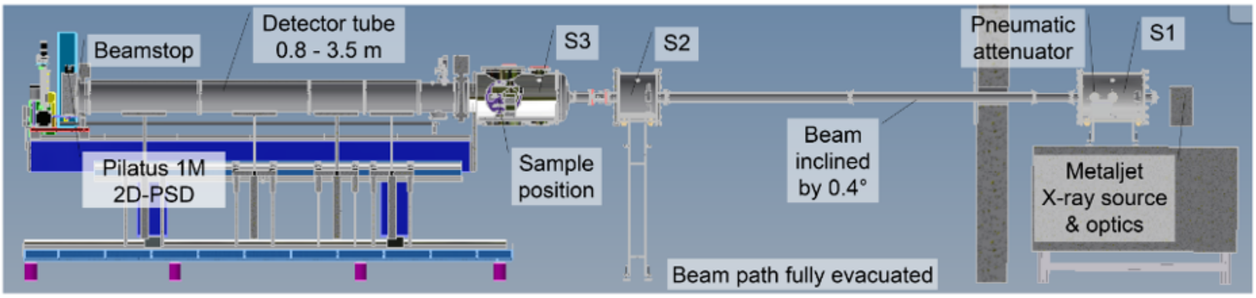

Figure 3.4: Sketch of GALAXI platform (figure taken from [30])

A further x-ray scattering technique based on Bragg's equation, is wide-angle x-ray scattering (WAXS). It is installed on the Gallium anode low-angle x-ray instrument (GALAXI) platform [30]. GALAXI can investigate structures in the order of 2 - 100 nm. Unlike small-angle x-ray scattering (SAXS), the distance from the sample to the detector for WAXS is shorter, and a wider range of angles is observed. Thus, WAXS is better for investigating crystalline material with long range order. A sketch of the GALAXI platform is shown in Figure 3.4.

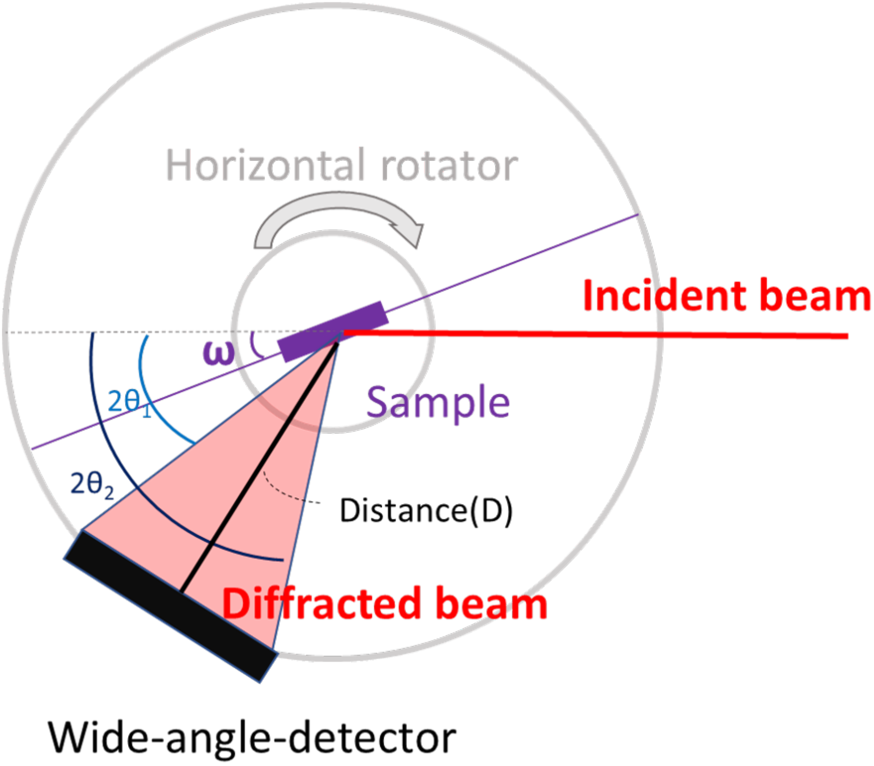

Figure 3.5: Sketch of the diffraction geometry in WAXS

GALAXI uses the Bruker AXS Metal jet X-ray source in Chamber S1 illustrated in Figure 3.4. An electron beam of 20μm height x 80μm width at 70 keV energy and 200 W power hits the liquid metal jet and X-rays are produced. The optics allow only the Ga K_α to pass and produce a monochromatic X-ray with the wavelength of 1.3414Å. The sample is mounted on a rotator in Chamber S3 which allows the sample to rotate horizontally with changing ω. The wide-angle detector is installed in the S3 chamber. As shown in Figure 3.5, the detector is placed at a certain distance (D) from the sample, for WAXS, this distance is around 85mm (D$\approx$85mm). Furthermore, the detector is placed at a certain angle to the sample, this angle is decided with regard to the peaks of interest. The detector is from DECTRIS, the length of the detector is 64mm with 1280 pixels on it. For a certain angle of the sample, the incident beam is diffracted into a region which will be collected by all the pixels of the detector with different 2θ. By rotating the sample, we can get a series of $\omega - 2\theta$ data which allows us to look into reciprocal space.

Chapter 4

Results and discussion

The samples of Fe_3O_4 thin films on YSZ substrates are grown by pulsed laser deposition (PLD). As there is a special matching of 3-fold Fe_3O_4 (111) thin films to the 4-fold YSZ (001) substrates, it is important to characterize the quality of the thin films. In section 4.2, the roughness of the thin films is measured. In section 4.3, 4.4 and 4.5, the in-plane and out-of-plane structure of Fe_3O_4(111) on YSZ(001) are presented.

4.1 Substrate preparation

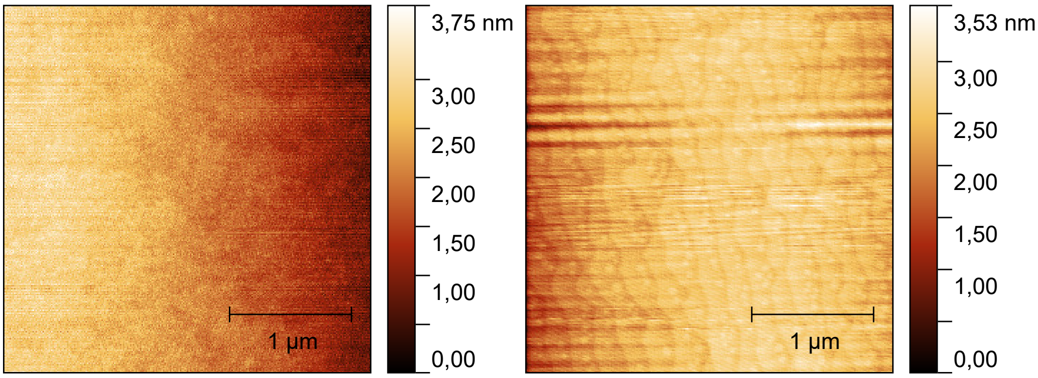

(a) Original **(b)** After annealing

Figure 4.1: Treatment to YSZ substrate: (a) original substrate, (b) substrate annealed at 1100°C for 8 h

The 10mmx10mmx0.5mm YSZ substrates from Crystec GmbH are annealed at 1100°C for 8 hours in order to achieve the better surface quality of the substrates. The different AFM images before and after annealing are shown in Figure 4.1. After annealing, the morphology changes to a terraced structure which indicates a smooth, well-ordered surface. The substrate is always considered as the main parameter for thin film growth which will also influence the crystllinity of the thin films.

4.2 Roughness-XRR

With X-Ray reflectometry, the roughness and thickness can be studied. The roughness of thin films indicates the quality of the thin films. As introduced in section 2.3.1, for incident angles below the critical angle (0.4°), we have total external reflection. Above the critical angle, the roughness of the thin films causes the exponential intensity reduction of the reflected wave as function of the incident angle. In other words, the intensity drops faster with increasing roughness.

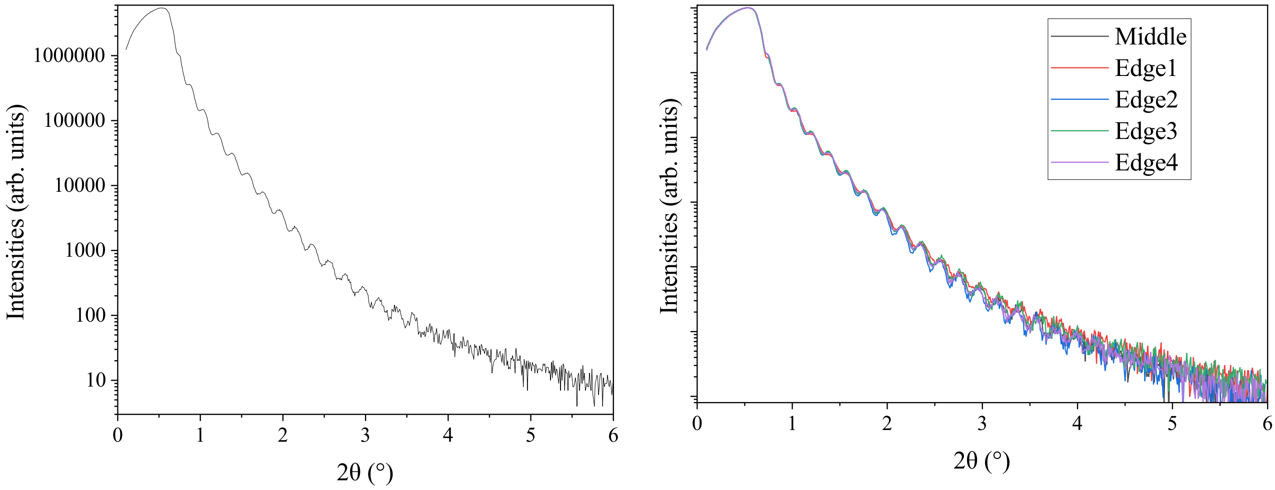

(a) **(b)**

Figure 4.2: (a) X-ray reflectivity, (b)XRR for the different position on same sample grown at 550°C

Besides of the roughness of the thin film surface, the thickness can also be concluded. Interference occurs between X-ray from the surface of the thin films and the refracted part of X-ray reflected from the interface. This interference causes oscillations of the reflectivity. These oscillations were found by Kiessing and named as Kiessing fringes[20]. By analyzing the period of the oscillations, we can calculate the film thickness. The thicker the film is, the shorter the period of the oscillations.

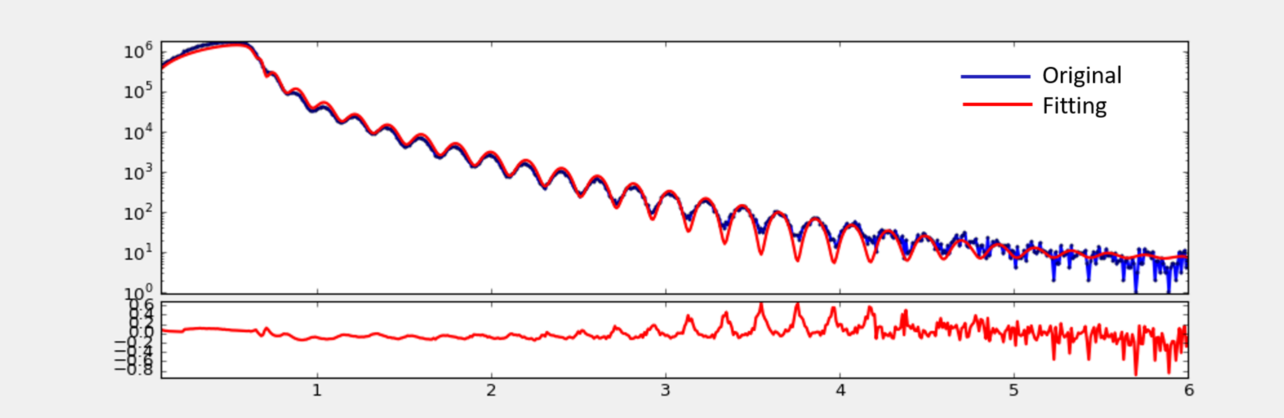

Figure 4.3: Fitting from GenX

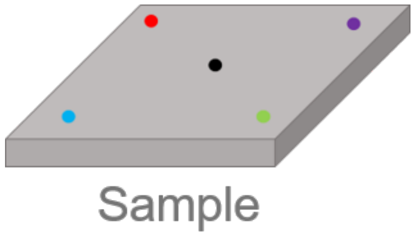

(a) XRR positions on sample

Position	Thickness/nm	Roughness/nm
Center	41.6 ± 0.1	0.64 ± 0.03
Edge 1	42.3 ± 0.9	0.82 ± 0.05
Edge 2	42.6 ± 0.8	0.85 ± 0.04
Edge 3	42.2 ± 0.7	0.85 ± 0.03
Edge 4	42.4 ± 1.5	0.85 ± 0.04

(b) Thickness and roughness calculated from the reflectivity of the Fe_3O_4 thin films from different position

Figure 4.4: XRR at different positions on the sample

Figure 4.2a shows the X-ray reflectivity of Fe_3O_4 thin films with T_{growth}=550°C in the range of 2θ=0.1°-6°. The measured reflectivity intensity data is fitted by GenX [16]. A fitting from GenX is shown in Figure 4.3. The thickness and roughness are found after the fitting. The calculated roughness at the center of the film is only around 0.64 nm, which indicates the good quality of thin films. Shown in Figure 4.2b, XRR measurements are done with the same 1cm x 1cm Fe_3O_4 on YSZ sample with different position. The positions are shown in Figure 4.4a. Results from different positions show a good consistency which indicates the homogeneous thin film. The accurate thickness and the roughness from different position of the thin films are shown in Figure 4.4b.

4.3 Out-of-plane structure: XRD

After confirmation with XRR results, we use X-ray diffraction (XRD) to analyze the out-of-plane crystallinity of the thin films using the Brucker-D8 instrument from PGI-7. Figure 4.5a shows the XRD scan of Fe_3O_4/YSZ system with the 2θ range from 10° to 90°. The substrate reflection peaks, YSZ (002) and YSZ (004), are strong and clear, which helps to align the beam. Using formula 2.2, the 2θ value of YSZ (002) is associated not only with the lattice constant, but also with the wavelength of the X-ray source. For Cu K_α, the wavelength is 1.54 Å, which causes the strongest peak around 34.9°, while the wavelength of Cu K_β is 1.39 Å, and causes the peak around 31.5°. Additionally, the four peaks of Fe_3O_4 in (111) direction all show up, while the other characteristic peaks of Fe_3O_4 do not. This indicates the Fe_3O_4 crystals are grown in the same out-of-plane direction. We conclude from this that Fe_3O_4 films grown at 550°C have a preferential orientation of (111) in the out-of-plane direction.

In order to investigate the local behavior, Figure 4.5b shows the XRD scan with the 2θ ranged from 30° to 40° around the YSZ (002) and Fe_3O_4 (222) reflection. First of all, there are clear Laue oscillations which indicates the good quality of the films as introduced in section 2.3.2. From the Laue oscillations, the thickness of the thin film can be calculated with the formula 2.3. As shown in table 4.1, the thickness of Fe_3O_4 thin films grown at 550°C calculated from Laue oscillation is around 40.33 nm. As mentioned in section 2.3.2, Laue oscillation is associated with the crystallinity. Thus, the thickness calculated from Laue oscillation is the thickness of the crystalline part of the film. There could be some amorphous dead layers in our thin film system and these would not contribute to the Laue oscillations. That could be the reason that the thickness calculated from Laue oscillation is

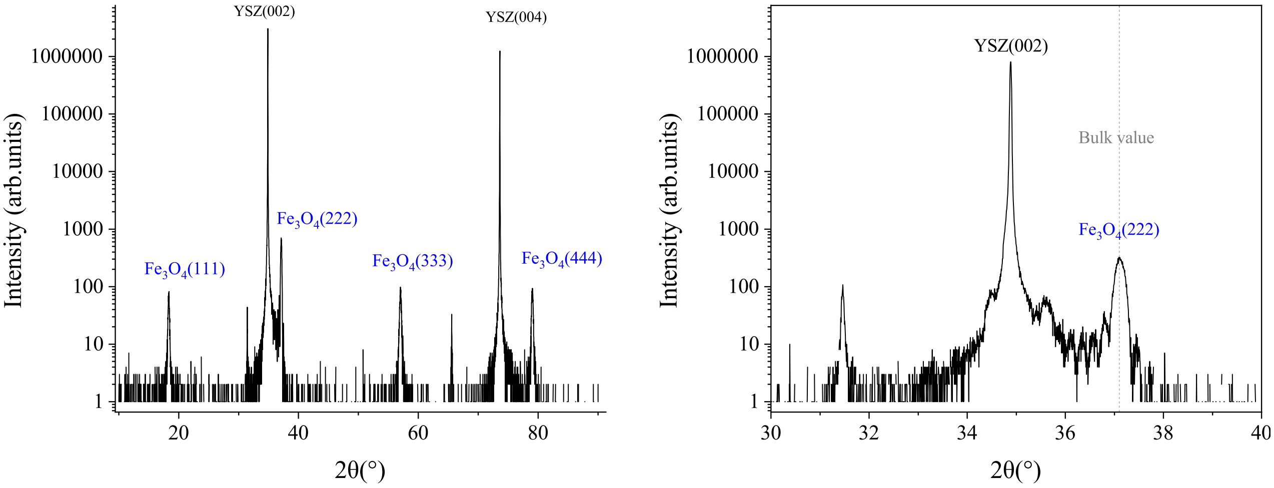

(a) XRD between 2θ=10°-90° **(b)** XRD between 2θ=30°-40°

Figure 4.5: Out-of-plane X-ray diffraction scans of Fe_3O_4 thin films grown at 550°C of (a) all reflection in the range of 2θ=10°-90° and (b) around Fe_3O_4 (222) reflection in the range of 2θ=30°-40°.

slightly smaller than it from XRR. However, the difference between the thickness of thin films and crystallinity is only around 1 nm, which indicates the good crystallinity of the entire film layer.

Method	Thickness/nm
XRR	41.6 ± 0.1
XRD laue oscillation	40.3 ± 0.6

Table 4.1: Thickness calculated from XRR and XRD

As mentioned in section 2.2, driven by the large mismatch, Fe_3O_4 tends to arrange in (111) plane on the YSZ (001) substrate, which can be noted as $(111)_{Fe_3O_4} \| (001)_{YSZ}$. As shown in Figure 4.5b, the bulk value of the Fe_3O_4 (222) peak is 2θ=37.07° (grey dashed line). With the help of Formula 2.2, we can calculate the bulk value of the interplanar spacing of the thin film in out-of-plane (d_{111}) direction.

$$d_{111,bulk} = \frac{n\lambda}{2sin\theta}$$

$$d_{111,bulk} = \frac{2 * 1.54\mathring{A}}{2 * sin(\frac{37.07°}{2})} = 4.8443\mathring{A}$$

Ideally, the Fe_3O_4 film grows relaxed which means the in-plane and out-of-plane interplanar spacing ($d_{10\bar{1}}, d_{111}$) should be equal to the bulk value.

As shown in Figure 4.5b, the peak of Fe_3O_4 shows a slight shift from the bulk value with 2θ=37.11°. The out-of-plane interpanar spacing can be calculated: $d_{111} = 4.8391 \pm 0.0061\mathring{A}$, which is comparable with the bulk value. This shows the good quality of Fe_3O_4 thin films, and that they are growing relaxed on the substrate.

4.4 In-plane: 4-Circle

According to the out-of-plane XRD patterns, the films are (111)-oriented as shown in Figure 4.5a. However, only the information of out-of-plane structure of thin films can be studied with the measurements of the Bruker D8 Diffractometer. In order to investigate the in-plane structure of Fe_3O_4 thin films, in-plane ϕ-scan (Azimuth scan) were performed using a 4-Circle instrument, which was introduced in section 3.3.

4.4.1 ϕ-scan of YSZ substrate

With changing ω and 2θ, different reflections can be obtained, which represents a family of planes in the crystal. With changing χ, we can reach different reflections in the same family. Here YSZ (220) is chosen to be observed. As shown in table 4.2, the χ value of all the possible reflections of YSZ (220) with respect to the c-axis (001) are calculated. When $\chi = 45°$, there are four possible reflections: (022), (202), $(0\bar{2}2)$ and $(\bar{2}02)$. These reflections with the same ω, 2θ and χ value can be measured individually with a ϕ-scan.

Reflection	(022)	(202)	$(0\bar{2}2)$	$(\bar{2}02)$	(220)	$(\bar{2}20)$	$(2\bar{2}0)$	$(\bar{2}\bar{2}0)$	$(20\bar{2})$	$(02\bar{2})$	$(\bar{2}0\bar{2})$	$(0\bar{2}\bar{2})$
$\chi(°)$	45	45	45	45	90	90	90	90	135	135	135	135

Table 4.2: χ of the reflections of (220) with the c-axis (001) of YSZ

As shown in Figure 4.6, the ϕ-scan around YSZ (220) is performed with $\omega = 25.39°$, $2\theta = 49.93°$, $\chi = 44.45°$. Four peaks differing by 90° which correspond to the four reflections show up. The strong and sharp peaks indicates the good crystallinity of the substrate.

This four-fold symmetry can also be explained by the crystal structure of YSZ. As introduced in section 2.2, YSZ crystal has a face centered cubic structure. The (220) plane symmetrically shows up every 90° because of the cubic structure. The sketch of YSZ (001) plane is drawn with VESTA as shown in Figure 2.2a [13].

4.4.2 ϕ-scan of Fe_3O_4 thin film

After confirmation of the four-fold in-plane symmetry of YSZ substrates, we study the in-plane structure of Fe_3O_4 by performing a ϕ-scan around Fe_3O_4 (220). The multiplicity of Fe_3O_4 (220) reflection is 12. The χ-values between every reflection and the norm perpendicular to the Fe_3O_4 (111) are calculated and shown in table 4.3. $\chi = 35.26°$ and $\chi = 144.74°$ are equivalent. Both of them have three reflections at $\chi = 35.26°$ or $\chi = 144.74°$. At $\chi = 90°$, there are six reflections, the pole figure of Fe_3O_4 (220) reflections is shown in Figure 6.1a.

The ϕ-scan around Fe_3O_4 (220) is performed with $\omega = 14.04°$, $2\theta = 30.07°$ and $\chi = 124.29°$ as shown in Figure 4.7a. The different χ value can be induced by the misalignment of the 4-Circle system

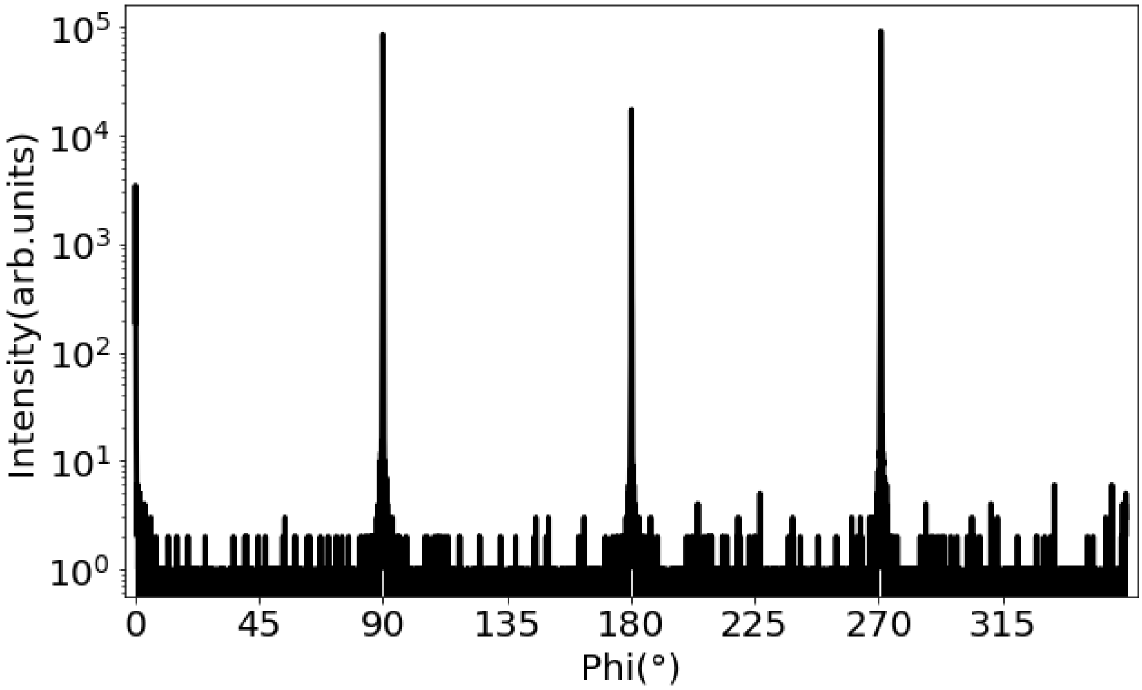

Figure 4.6: ϕ-scan of YSZ (220) with $\chi = 44.45°$

Reflection	(220)	(202)	(022)	$(\bar{2}\bar{2}0)$	$(\bar{2}0\bar{2})$	$(0\bar{2}\bar{2})$
$\chi(°)$	35.26	35.26	35.26	144.74	144.74	144.74
Reflection	$(\bar{2}20)$	$(\bar{2}02)$	$(0\bar{2}2)$	$(2\bar{2}0)$	$(20\bar{2})$	$(02\bar{2})$
$\chi(°)$	90	90	90	90	90	90

Table 4.3: χ of the reflections of (220) with the c-axis (111) of Fe_3O_4

which is not fully understood here. Instead of 3, 12 reflections are found. In order to understand the 12 peaks, we need to look into the crystal structure of Fe_3O_4 aligned in the [111] direction and (111) plane.

As shown in Figure 2.2c, the bulk Fe_3O_4 crystal align in the (111) plane shows a three-fold symmetry which can explained by the three symmetric reflections $(\bar{2}\bar{2}0)$, $(\bar{2}0\bar{2})$ and $(0\bar{2}\bar{2})$ at $\chi = 144.74°$. These three reflections are marked in red in Figure 4.7a. The multiple peaks in the ϕ-scan can indicate the presense of domains in crystals which is also discussed by Yingfen Wei, et cl. (2008) and KwaDwo Konadu Ansah-Antwi et cl (2015) [21][22]. Thus, we can conclude that the 12 peaks are caused by four unique crystallographic domains of Fe_3O_4 (111) on YSZ (001) which is shown by different color in Figure 4.7a.

Yingfen Wei assumes the crystal domains are rotated 90° with respect to each other which is induced by the occupation on the four-fold symmetry of a (001)-oriented cubic surface . They confirmed this assumption with a transmission electron microscope (TEM) measurement.

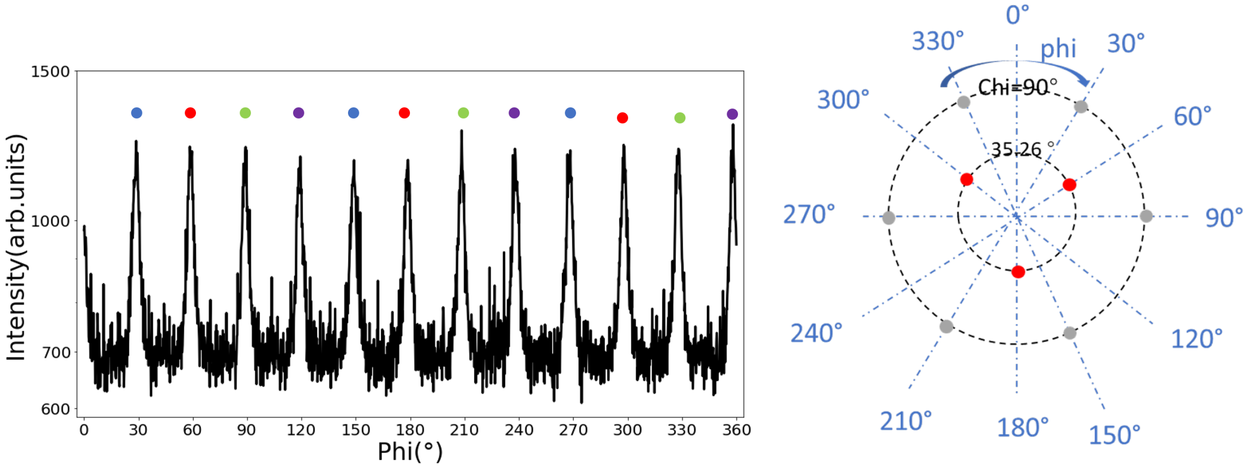

(a) Fe_3O_4 (220) with $\chi = 124.292°$ **(b)** Pole figure of Fe_3O_4 (220) reflections

Figure 4.7: ϕ scan at $\chi = 124.29°$ and theoretical pole figure of Fe_3O_4 (220) reflections

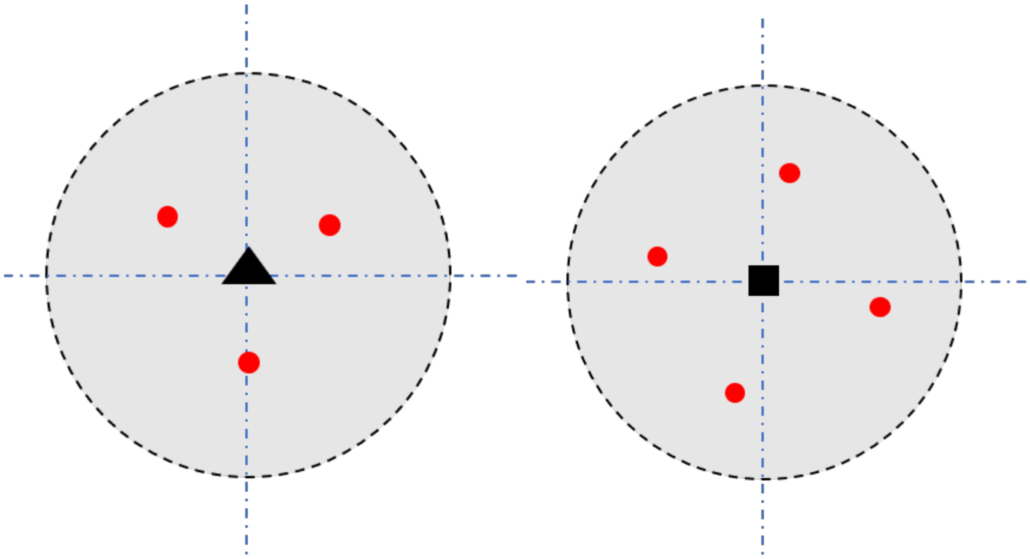

(a) Three-fold **(b)** Four-fold

Figure 4.8: Symmetry of 3-fold and 4-fold rotation axis

Based on the reference, we can draw definite inferences: the 12 reflections in Figure 4.7a indicates there are four domains with different but well-defined in-plane orientations. The most likely reason for the four domains may be consistent with the work of Yingfen Wei (2018)[21].

As shown in Figure 2.2a, the (001) plane of YSZ has a square structure, however, the (111) plane of Fe_3O_4 shows a hexagonal lattice of atoms (Figure 2.2c). Thus, induced by the cubic substrate crystal structure, there are four possible growth orientations (differing by 90°) as shown in Figure 4.9. As shown in Figure 4.8, magnetite thin film has a 3-fold symmetry and the substrate has a 4-fold symmetry. The 4-fold symmetry will produce 4 equivalent reflections of each from the thin film by 90°. These rotations further result in the different in-plane direction of Fe_3O_4 illustrated by the direction of the golden triangles depicted in Figure 4.9.

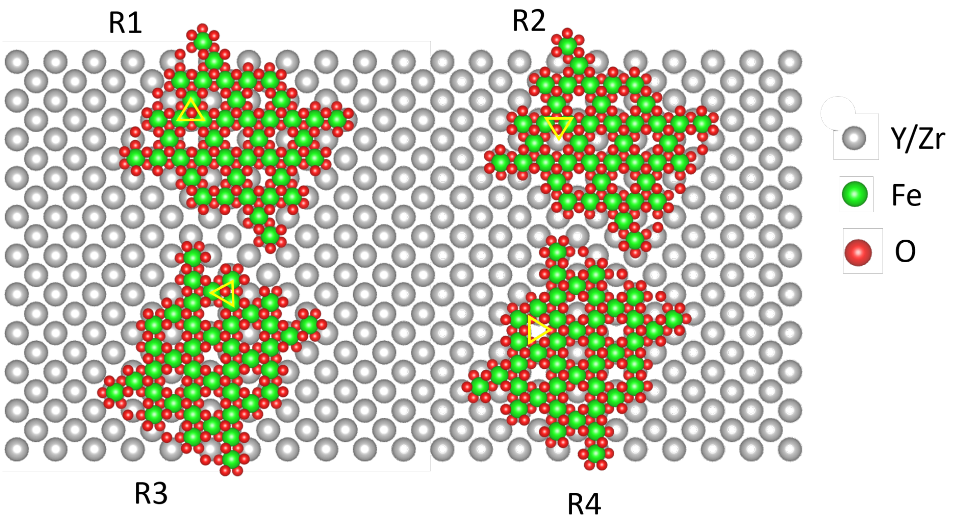

Figure 4.9: Fe_3O_4 (111) plane on YSZ (001) plane with four different orientation (R1,R2, R3 and R4) with respect to 90°.

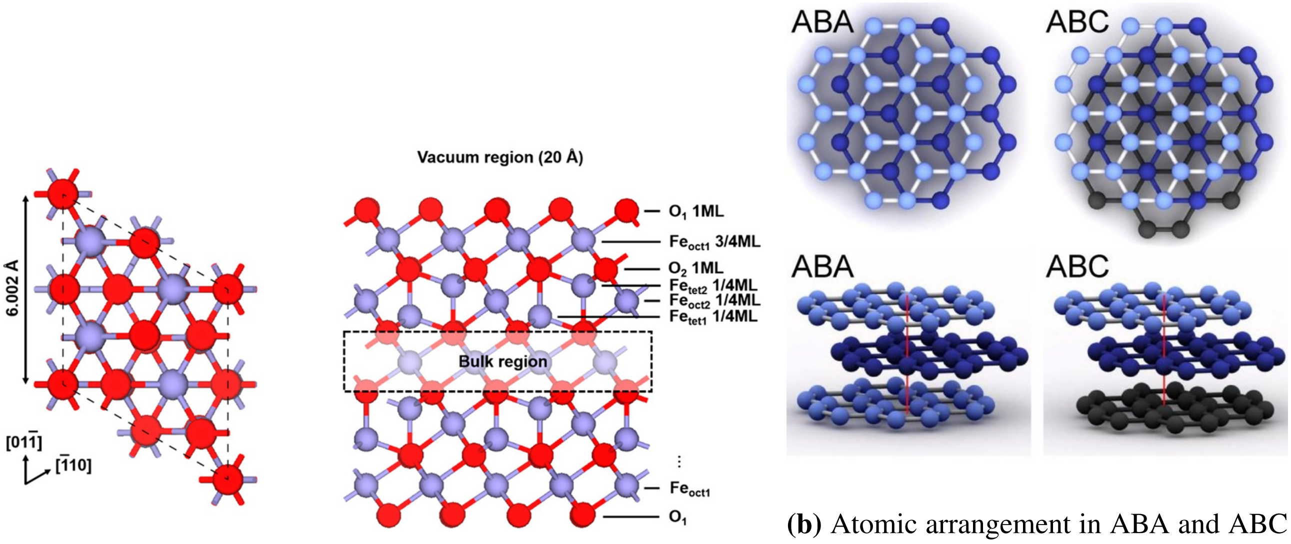

(a) Fe_3O_4 (111) slab model taken from [1]

(b) Atomic arrangement in ABA and ABC stacking [23]

Figure 4.10: Top and side views of Fe_3O_4 (111) slab model and atomic arrangement in ABA and ABC stacking

In summary, there are two main parameters influencing the number of reflections in the ϕ-scan shown in Figure 4.7a:

1) The three reflections caused by the three-fold symmetry of Fe_3O_4 crystal oriented in (111).
2) The four growth orientation differing by 90° caused by the hexagonal lattice of Fe_3O_4 on a cubic substrate.

Furthermore, the different stacking modes of Fe and O layers inside Fe_3O_4 can also influence the domain. Four different domains of iron oxide are also discussed by Ivan Ermanoski (2013) :the four domains of FeO(111) on YSZ(001) are caused by both occupation of a hexagonal overlayer on a square substrate and the different stacking mode of iron oxide [24].

In the study from Noh Junghyun (2015), the stacking sequence of Magnetite (111) is studied [1]. As shown in Figure 4.10a, there are four Fe teminations which can present two different Fe sublayers:

1) A dense monolayer with all octahedrally coordinated Fe in the same plane (Fe$_{oct1}$).
2) A sublayer contains three distinct low-density monolayers with Fe in both octahedral and tetrahedral sites (Fe$_{tet2}$-Fe$_{oct2}$-Fe$_{tet1}$).

These two sublayers are alternating stacking which can also result in different domains. The influence of stacking mode will be a good research direction in the future.

4.4.3 Uncertainty of adjustment

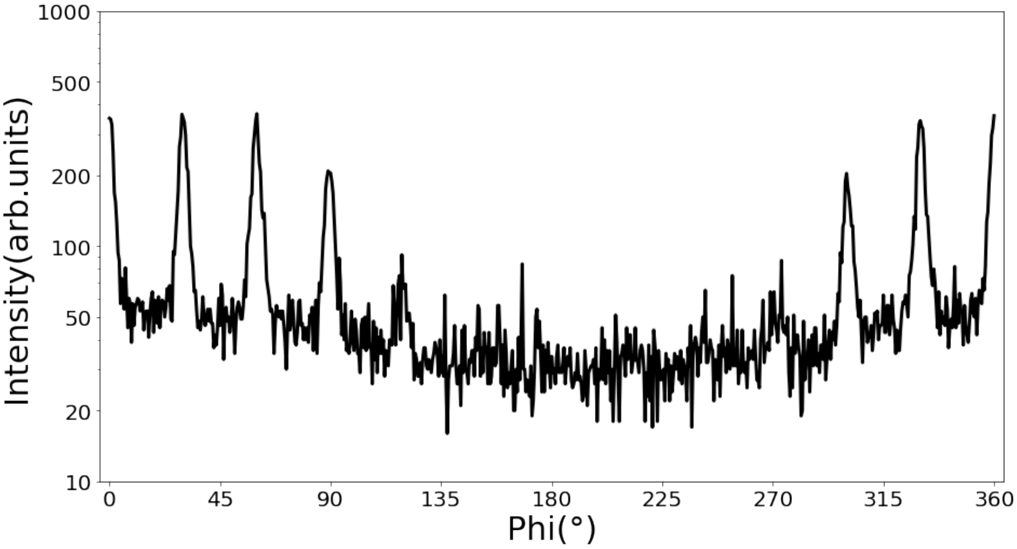

Figure 4.11: ϕ scan around Fe$_3$O$_4$(226) at $\chi = 35.40°$

We observed a systematic error of the 4-Circle instrument during adjustment of the position of samples. According to the user manual, we have to arrange the X-ray beam to go through the center of rotation [25]. Thus, we have to adjust the position of the samples (p_z) by hand and calibrate the position where the X-ray goes through the center of the film. This manual adjustment can bring uncertainty into the measurements.

As shown in Figure 4.11, we performed a ϕ-scan around the (226) reflection with $\chi = 35.40$. We observed the different intensities for these 12 peaks which is induced by the misalignment between the rotation center of thin films and the X-rays. In order to obtain quantifiable data from the measurements, we need to adjust it carefully. In the future, fine adjustment will be possible with a fully motorized system.

4.5 WAXS

Wide angle X-ray scattering is a good method to study the crystallinity and the lattice constant in both in-plane and out-of-plane directions [26]. The 2θ and ω values obtained in the measurements can be converted to Q_x, Q_z and Q with the formula below with $\lambda = 1.34\mathring{A}$:

$$Q_x = \frac{2\pi}{\lambda} * (cos(\omega) - cos(2\theta - \omega))$$

$$Q_z = \frac{2\pi}{\lambda} * (sin(\omega) + sin(2\theta - \omega))$$

$$Q = \sqrt{Q_x^2 + Q_z^2}$$

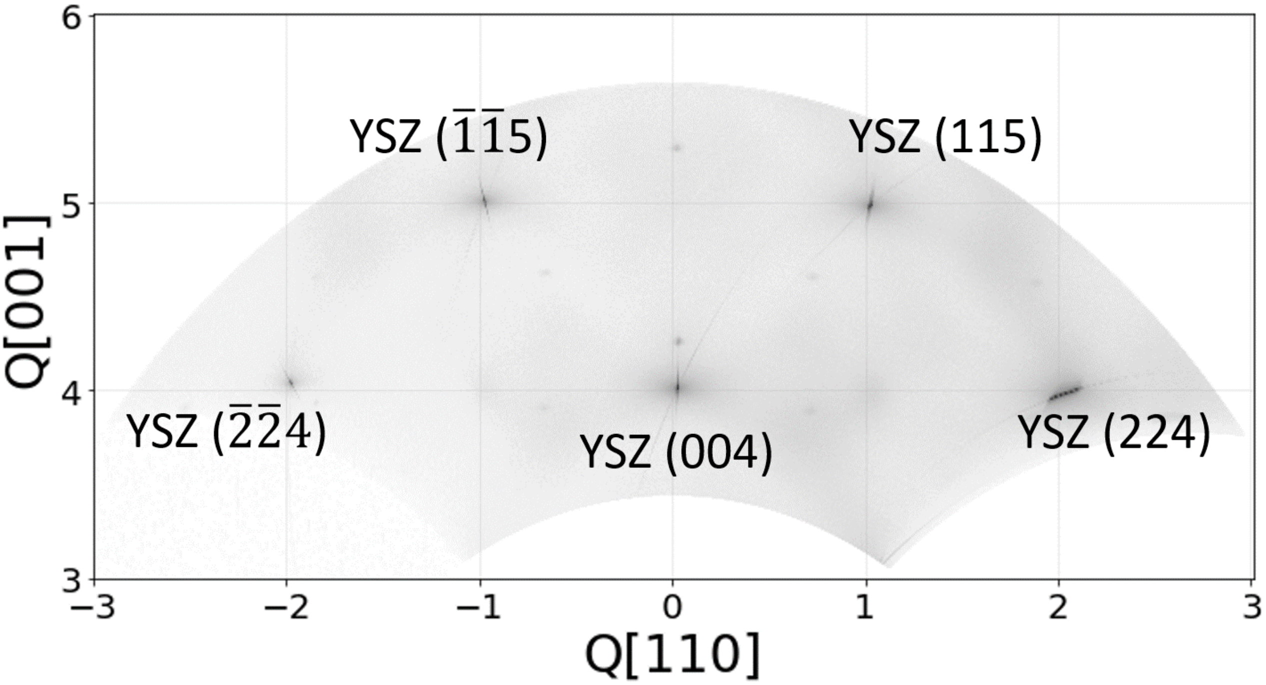

Figure 4.12: Reciprocal space mapping with horizontal axis along [001] and vertical axis along [110] in reciprocal lattice units of the substrate

The reciprocal space intensities are further calculated in reciprocal lattice units of the YSZ substrates with horizontal axis along [001] direction and the vertical axis along [110] direction with the equations:

$$h = Q_x * a_{ip}/(2\sqrt{1^2 + 1^2 + 0^2}\pi)$$

$$l = Q_z * c_{oop}/(2\sqrt{0^2 + 0^2 + 1^2}\pi)$$

As shown in Figure 4.12, we can index the five strong peaks of YSZ substrates. The other weak peaks are from Fe_3O_4.

The diffraction patterns indicate the different crystalline state. [27]. As shown in Figure 4.13, a single crystal shows a spot-like diffraction pattern due to the periodicity repetition of the crystal unit cell.

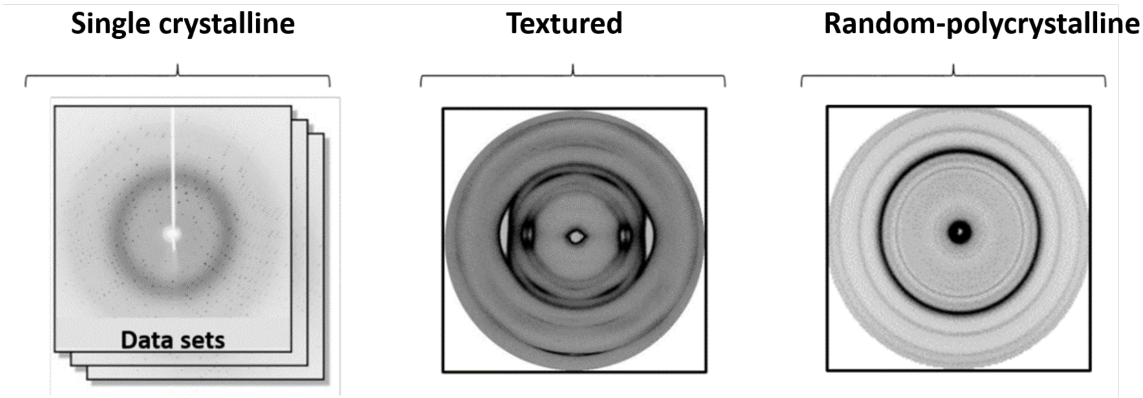

Figure 4.13: Diffraction patterns of single crystal, textured materials and ranfom-polycrystalline, figure taken from [27]

Fibers with preferential orientation in in-plane and out-of plane show arcs along the preferential orientation. Polycrystalline materials shows a circle pattern induced by the orientation of the small single crystal inside polycrystalline materials in all directions. Thus, the spot-like intensity distribution in Figure 4.12 indicates the single crystallinity of our film.

In order to calculate the reciprocal space unit of Fe_3O_4, the in-plane and out-of-plane information is needed. According to the powder diffraction results in Figure 4.5, the Q_z axis of Fe_3O_4 reciprocal space should be perpendicular to [111]. However, as the in-plane information is unknown, it's difficult to index the peaks. A possible way to index the peaks of Fe_3O_4 is discussed in appendix A. The data analyzation process is still on-going, which might conclude the twining state of the thin films.

Chapter 5

Summary

The aim of this project is to investigate the in-plane structure of Fe_3O_4 (111) magnetite thin films on YSZ (001) substrates deposited by PLD.

First, in order to check the thin film quality, we characterized the thin film roughness by using XRR. The low roughness indicates thin films with good surface quality.

From XRD measurements, only four peaks of Fe_3O_4 in the same direction of (111) are observed. It indicates the single growth-orientation of Fe_3O_4 thin films. Furthermore, the interplanar spacing between (111) plane is comparable the bulk value which reveals the relaxed states in Fe_3O_4 thin films.

The in-plane structure is studied by ϕ-scan. Instead of 3, we observed 12 reflections from the ϕ-scan around Fe_3O_4 (220). These 12 reflections strongly indicate four in-plane domains which can be induced by both the substrate and the stacking mode.

With WAXS, the structure in both in-plane and out-of-plane can be investigated. The spotted-like intensity distribution of Fe_3O_4 thin films indicates the single crystallinity in both directions.

Chapter 6

Outlook

In this project, we characterized the properties of Fe_3O_4 (111) thin films on YSZ (001) substrates and observed different domains in the in-plane direction.

As introduced in section 3.3, the domains structure can be observed by the transmission electron microscopy (TEM) including the region and the angle between different domains [28]. With the 4-Circle instrument, a ϕ-scan with only one χ is done, the pole figure is shown in Figure 6.1a. This is not enough to study the whole structure over the film. In the study from Yingfen Wei (2018), ϕ-scans 0 - 360° with χ=0-90° are done and the pole figure as shown in Figure 6.1b provides the information of other weak peaks in other χ angles indicating the possible different orientations within the thin films. Thus, a full pole figure can offer the information about the poly/ single crystallinity.

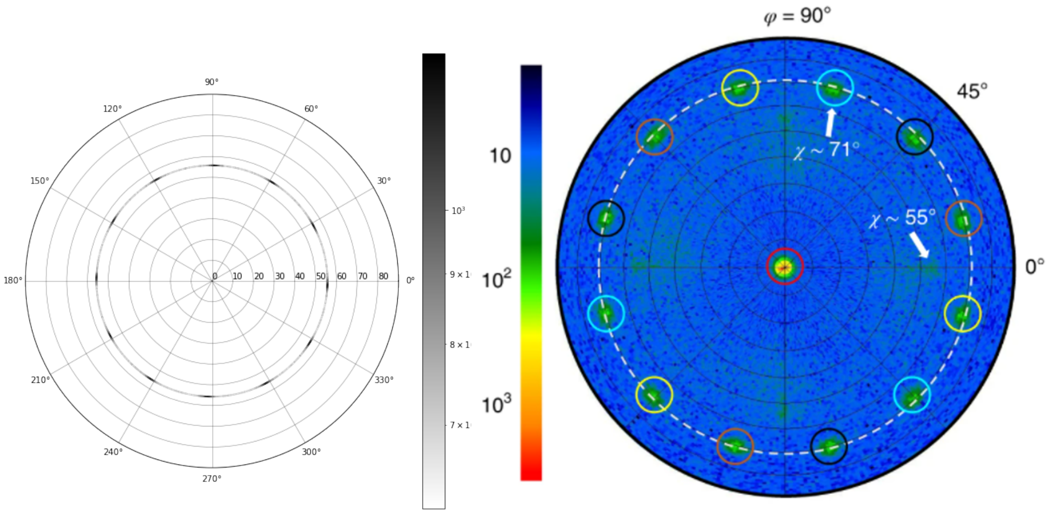

(a) Pole figure of Fe_3O_4 (220)

(b) Pole figure of a cubic crystal aligned in (111) plane with 4 domains, figure taken from [21]

Figure 6.1: Pole figures

Further, by measuring multiple peaks of Fe_3O_4 and constructing the UB Matrix, the atomic information of the thin film can be drawn. Thus, the complete crystal lattice can be derived.

The data of WAXS will be further studied with the help of hexagonal coordinate system which will offer us the information and perhaps indication of a twinning state.

Last but not least, with WAXS we can study the in-plane and out-of-plane information in the bulk thin film. GIWAXS (Grazing angle wide-angle X-ray scattering) can in contrast, provide the information only of the surface. Thus, using these two methods, we can explore the different properties at both surface and interface to study the in-plane structure of Fe_3O_4 (111).

Appendix A

Indexing the Fe_3O_4 reflection peaks in WAXS

Shown in Figure A.1, the films peaks are marked with circles. As discussed in section 3.4, the Q_z of Fe_3O_4 is along [111] direction. Thus, we can index (444) and (555) peaks.

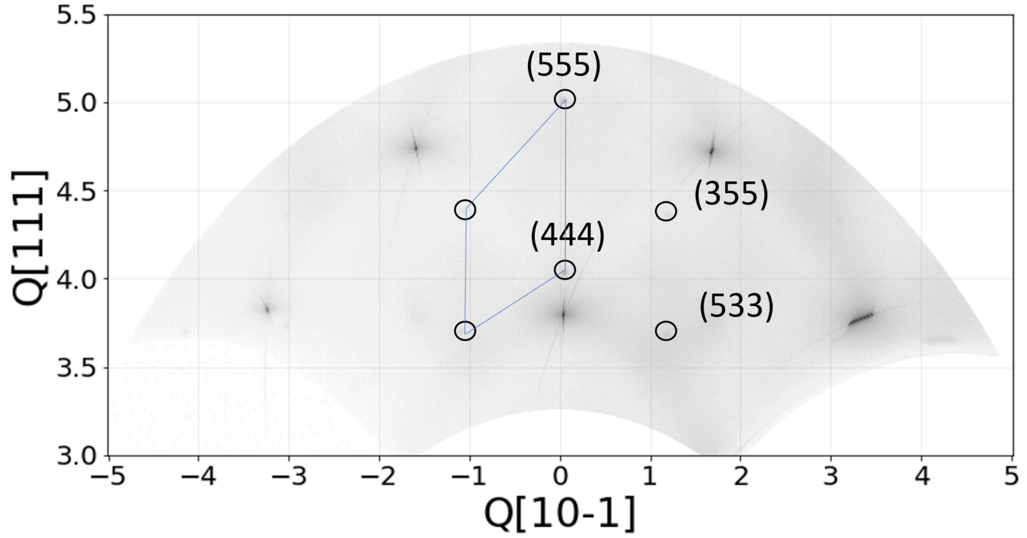

Figure A.1: Reciprocal space mapping with horizontal axis along [111] and vertical axis along $[10\bar{1}]$ in reciprocal lattice units of Fe_3O_4

Reflection	$Q_{bulk}(\mathring{A}^{-1})$	$Q_{measured}(\mathring{A}^{-1})$
(533)	4.9079	4.9318
(444)	5.1854	5.2295
(553)	5.7489	5.7901
(555)	6.4817	6.4932

Table A.1: Theoretical bulk Q-value and the calculated Q-value from the measurements of Fe_3O_4 reflections

As the in-plane structure is needed for indexing the peaks of Fe_3O_4, we can index the other peaks of Fe_3O_4 by comparing the Q value with the bulk value. The Q value of bulk value and of measured data can be calculated with $Q = \frac{4\pi sin(\theta)}{\lambda}$, with different bulk or measured θ-values. With the comparison of Q values as shown in table A.1, we can index the (355) and (533) film peaks in Figure A.1. The vertical axis direction in Figure A.1 is discussed in appendix B.

However, we know that Fe_3O_4 (111) should be properly indexed on a hexagonal coordinate system as marked with blue lines in FigureA.1. It would involve transforming the cubic coordinates to that of a hexagonal system, which is beyond the scope of this project [17].

Appendix B

Reciprocal space of Fe_3O_4

Confrimed by XRD, Fe_3O_4 thin films align along [111] direction in out-of-plane which means Q_x of Fe_3O_4 is parallel to [111]. In order to figure out the in-plane direction, we assume Q_x parallel to [uvw], we can project the Q value of certain reflection [hkl] on the [uvw] direction with θ equals to the angle between the reflection [hkl] and [uvw]:

$$Q_x = Q * cos\theta$$

$$Q_x = Q * \frac{h*u + k*v + l*w}{\sqrt{u^2+v^2+w^2} * \sqrt{h^2+k^2+l^2}}$$

As introduced in section 3.4, Q, Q_x and Q_z can be calculated from the measured 2θ and ω data as shown in table B.1.

Reflection	$Q(\AA^{-1})$	$Q_x(\AA^{-1})$	$Q_z(\AA^{-1})$
(533)	4.9318	1.1858	4.7871
(444)	5.2295	0	5.2295
(553)	5.7901	1.1986	5.6647
(555)	6.4932	-0.0303	6.4931

Table B.1: χ of the reflections of (220) with the c-axis (111) of Fe_3O_4

Thus, we can combine the equations which are mentioned before and make a sequence of equations:

$$Q_{x,533} = Q * \frac{5u + 3v + 3w}{\sqrt{u^2+v^2+w^2} * \sqrt{5^2+3^2+3^2}} = 1.1858$$

$$Q_{x,553} = Q * \frac{5u + 5v + 3w}{\sqrt{u^2+v^2+w^2} * \sqrt{5^2+5^2+3^2}} = 1.1986$$

Thus, we can get:

$$5u + 3v + 3w = \frac{1.1858 * \sqrt{43}}{4.9318} * \sqrt{u^2+v^2+w^2}$$

$$5u+5v+3w=\frac{1.1986*\sqrt{59}}{5.7901}*\sqrt{u^2+v^2+w^2}$$

$$\frac{5u+3v+3w}{5u+5v+3w}=\frac{1.1858*\sqrt{43}}{4.9318}*\frac{5.7901}{1.1986*\sqrt{59}}$$

$$\frac{5u+3v+3w}{5u+5v+3w}=0.99\approx 1$$

$$5u+3v+3w=5u+5v+3w$$

Thus $v=0$, and Q_x is parallel to [u0w]. Q_x is perpendicular to Q_z and Q_z is parallel to [111]:

$$u*1+0*1+w*1=0$$

$$u=-w$$

Thus, Q_x is parallel to $[10\bar{1}]$, the Q_x and Q_z values of Fe_3O_4 and YSZ are parallel to different directions, which can be represented as $(111)\langle 10\bar{1}\rangle_{Fe_3O_4}\|(001)\langle 110\rangle_{YSZ}$.

Acknowledgments

My deepest gratitude goes first and foremost to Prof. Dr. Thomas Brückel, my main supervisor, for giving me the chance to work at the ”Jülich Center for Neutron Science (JCNS-2), Forschungszentrum Jülich GmbH” and instructive suggestions on my thesis. I am thankful to Prof. Dr. Regina Dittmann for being willing to be my second main supervisor and for the useful suggestions.

I am profoundly grateful to Dr. Mai Hussein and Dr. Connie Bednarski-Meinke for being my supervisors, for the constant encouragement and guidance, for imparting me with plenty of knowledge and expertise, for the English language corrections and for walking me through all the stages of the writing of this thesis. The completion of this thesis would not have been possible without their patient instruction, insightful criticism and expert guidance.

My sincere thanks go to Dr. Emmanuel Kentzinger, Dr. Oleg Petracic, Dr. Shibabrata Nandi, Dr. Ulrich Rücker and Berthold Schmitz, for the introduction to and suggestions for the devices used throughout this thesis project. My special thanks go to Dr. Asmaa Qdemat, Dr. Paul Zakalek for the helping to conduct the measurements.

I would like to express my heartfelt gratitude to Prof. Karen Friese, Dr. Artur Gregor Glavic, Dr. Felix Gunkel, Dr. Steffen Tober for the useful discussion.

I would also like to thank all my other colleagues at JCNS-2, especially the thin film group, who are always polite and willing to help and always create a creative and delightful working atmosphere.

Last but not least, my greatest thanks would go to my beloved family, Mr. Hong Xu and Mrs. Huimin Tian and my boyfreiend, Mr. Julian Lindlar, have always been supportive of me, and have constantly motivated and encouraged me during my work. I also owe my sincere gratitude to my friends for their loving consideration of me.

List of Figures

List of Tables

Bibliography

[1] Junghyun Noh, Osman I Osman, Saadullah G Aziz, Paul Winget, and Jean-Luc Bredas. Magnetite Fe_3O_4 (111) surfaces: impact of defects on structure, stability, and electronic properties. *Chemistry of Materials*, 27(17):5856–5867, 2015.

[2] Scott A. Chambers. Epitaxial growth and properties of thin film oxides. *Surface Science Reports*, 39(5):105–180, 2000.

[3] Xionghua Liu, Chun-Fu Chang, Aurora Diana Rata, Alexander Christoph Komarek, and Liu Hao Tjeng. Fe3o4 thin films: controlling and manipulating an elusive quantum material. *npj Quantum Materials*, 1(1):1–5, 2016.

[4] Shailja Tiwari, Ram Prakash, RJ Choudhary, and DM Phase. Oriented growth of Fe_3O_4 thin film on crystalline and amorphous substrates by pulsed laser deposition. *Journal of Physics D: Applied Physics*, 40(16):4943, 2007.

[5] B Stanka, W Hebenstreit, U Diebold, and SA Chambers. Surface reconstruction of Fe_3O_4 (001). *Surface science*, 448(1):49–63, 2000.

[6] A Barbieri, W Weiss, MA Van Hove, and GA Somorjai. Magnetite Fe_3O_4 (111): surface structure by LEED crystallography and energetics. *Surface Science*, 302(3):259–279, 1994.

[7] Michail Fonin, Yu S Dedkov, Rossitza Pentcheva, Ulrich Rüdiger, and Gernot Güntherodt. Magnetite: a search for the half-metallic state. *Journal of Physics: Condensed Matter*, 19(31):315217, 2007.

[8] ME Fleet. The structure of magnetite. *Acta Crystallographica Section B: Structural Crystallography and Crystal Chemistry*, 37(4):917–920, 1981.

[9] Malcolm W Chase. NIST-JANAF thermochemical tables for oxygen fluorides. *Journal of physical and chemical reference data*, 25(2):551–603, 1996.

[10] George F Harrington and José Santiso. Back-to-basics tutorial: X-ray diffraction of thin films. *Journal of Electroceramics*, pages 1–23, 2021.

[11] Ivan Vesselinov Markov. *Crystal growth for beginners: fundamentals of nucleation, crystal growth and epitaxy*. World scientific, 2016.

[12] Lambert Ben Freund and Subra Suresh. *Thin film materials: stress, defect formation and surface evolution*. Cambridge university press, 2004.

[13] Koichi Momma and Fujio Izumi. VESTA 3 for three-dimensional visualization of crystal, volumetric and morphology data. *Journal of applied crystallography*, 44(6):1272–1276, 2011.

[14] Mai Hussein Abdalla Hamed. Interface functionalization of magnetic oxide Fe_3O_4/$SrTiO_3$ heterostructures. Technical report, Elektronische Eigenschaften, 2021.

[15] George F Harrington, Andrea Cavallaro, David W McComb, Stephen J Skinner, and John A Kilner. The effects of lattice strain, dislocations, and microstructure on the transport properties of YSZ films. *Physical Chemistry Chemical Physics*, 19(22):14319–14336, 2017.

[16] Matts Björck and Gabriella Andersson. Genx: an extensible x-ray reflectivity refinement program utilizing differential evolution. *Journal of Applied Crystallography*, 40(6):1174–1178, 2007.

[17] Charles Kittel. Introduction to solid state physics Eighth edition. 2021.

[18] YK Vayunandana Reddy, Jérôme Wolfman, Cécile Autret-Lambert, Monique Gervais, and François Gervais. Strain relaxation of epitaxial $(Ba_{0.6}Sr_{0.4})(Zr_{0.3}Ti_{0.7})O_3$ thin films grown on $SrTiO_3$ substrates by pulsed laser deposition, 2010.

[19] Paul F Fewster. Reciprocal space mapping. *Critical Reviews in Solid State and Material Sciences*, 22(2):69–110, 1997.

[20] Heinz Kiessig. Untersuchungen zur Totalreflexion von Röntgenstrahlen. *Annalen der Physik*, 402(6):715–768, 1931.

[21] Yingfen Wei, Pavan Nukala, Mart Salverda, Sylvia Matzen, Hong Jian Zhao, Jamo Momand, Arnoud S Everhardt, Guillaume Agnus, Graeme R Blake, Philippe Lecoeur, et al. A rhombohedral ferroelectric phase in epitaxially strained $Hf_{0.5}Zr_{0.5}O_2$ thin films. *Nature materials*, 17(12):1095–1100, 2018.

[22] KwaDwo Konadu Ansah-Antwi, Chew Beng Soh, Hongfei Liu, and Soo Jin Chua. Growth optimization and characterization of GaN epilayers on multifaceted (111) surfaces etched on Si (100) substrates. *Journal of Vacuum Science & Technology A: Vacuum, Surfaces, and Films*, 33(6):061517, 2015.

[23] Tataiana Latychevskaia, Seok-Kyun Son, Yaping Yang, Dale Chancellor, Michael Brown, Servet Ozdemir, Ivan Madan, Gabriele Berruto, Fabrizio Carbone, Artem Mishchenko, et al. Stacking transition in rhombohedral graphite. *Frontiers of Physics*, 14(1):1–7, 2019.

[24] Ivan Ermanoski and G.L. Kellogg. Real-time observations of ultra-thin iron oxide film growth on oxygen-deficient YSZ(001). *Surface Science*, 614:1–11, 2013.

[25] Certified Scientific Software. *SPEC X-Ray Diffraction Software*.

[26] Kris Frost, Daniel Kaminski, Gemma Kirwan, Edmond Lascaris, and Robert Shanks. Crystallinity and structure of starch using wide angle x-ray scattering. *Carbohydrate Polymers*, 78(3):543–548, 2009.

[27] Teresa Sibillano, Alberta Terzi, Liberato De Caro, Massimo Ladisa, Davide Altamura, Anna Moliterni, Rocco Lassandro, Francesco Scattarella, Dritan Siliqi, and Cinzia Giannini. Wide angle x-ray scattering to study the atomic structure of polymeric fibers. *Crystals*, 10(4):274, 2020.

[28] Chengliang Lu, Hakan Deniz, Xiang Li, Jun-Ming Liu, and Sang-Wook Cheong. Continuous magnetoelectric control in multiferroic $DyMnO_3$ films with twin-like domains. *Scientific Reports*, 6:20175, 02 2016.

[29] Artur Glavic. *Multiferroicity in oxide thin films and heterostructures*, volume 45. Forschungszentrum Jülich, 2012.

[30] Emmanuel Kentzinger, Margarita Krutyeva, and Ulrich Rücker. Galaxi: Gallium anode low-angle x-ray instrument. *Journal of large-scale research facilities JLSRF*, 2:61, 2016.